NASA/TM—2006-214359

Three-Dimensional Field Solutions for Multi-Pole Cylindrical Halbach Arrays in an Axial Orientation

William K. Thompson
Glenn Research Center, Cleveland, Ohio

September 2006

NASA STI Program . . . in Profile

Since its founding, NASA has been dedicated to the advancement of aeronautics and space science. The NASA Scientific and Technical Information (STI) program plays a key part in helping NASA maintain this important role.

The NASA STI Program operates under the auspices of the Agency Chief Information Officer. It collects, organizes, provides for archiving, and disseminates NASA's STI. The NASA STI program provides access to the NASA Aeronautics and Space Database and its public interface, the NASA Technical Reports Server, thus providing one of the largest collections of aeronautical and space science STI in the world. Results are published in both non-NASA channels and by NASA in the NASA STI Report Series, which includes the following report types:

- TECHNICAL PUBLICATION. Reports of completed research or a major significant phase of research that present the results of NASA programs and include extensive data or theoretical analysis. Includes compilations of significant scientific and technical data and information deemed to be of continuing reference value. NASA counterpart of peer-reviewed formal professional papers but has less stringent limitations on manuscript length and extent of graphic presentations.

- TECHNICAL MEMORANDUM. Scientific and technical findings that are preliminary or of specialized interest, e.g., quick release reports, working papers, and bibliographies that contain minimal annotation. Does not contain extensive analysis.

- CONTRACTOR REPORT. Scientific and technical findings by NASA-sponsored contractors and grantees.

- CONFERENCE PUBLICATION. Collected papers from scientific and technical conferences, symposia, seminars, or other meetings sponsored or cosponsored by NASA.

- SPECIAL PUBLICATION. Scientific, technical, or historical information from NASA programs, projects, and missions, often concerned with subjects having substantial public interest.

- TECHNICAL TRANSLATION. English-language translations of foreign scientific and technical material pertinent to NASA's mission.

Specialized services also include creating custom thesauri, building customized databases, organizing and publishing research results.

For more information about the NASA STI program, see the following:

- Access the NASA STI program home page at *http://www.sti.nasa.gov*

- E-mail your question via the Internet to *help@sti.nasa.gov*

- Fax your question to the NASA STI Help Desk at 301–621–0134

- Telephone the NASA STI Help Desk at 301–621–0390

- Write to:
  NASA STI Help Desk
  NASA Center for AeroSpace Information
  7121 Standard Drive
  Hanover, MD 21076–1320

NASA/TM—2006-214359

Three-Dimensional Field Solutions for Multi-Pole Cylindrical Halbach Arrays in an Axial Orientation

William K. Thompson
Glenn Research Center, Cleveland, Ohio

National Aeronautics and
Space Administration

Glenn Research Center
Cleveland, Ohio 44135

September 2006

Acknowledgments

The author gratefully acknowledges Dennis J. Eichenberg, Jeffrey Juergens, and Dawn C. Emerson, NASA Glenn Research Center, for assistance with the development of the analytical models; Christopher A. Gallo, NASA Glenn, for contributions to the graphics; and Mark Christinin, Ansoft, Inc., for assistance with the finite-element model.

This work was sponsored by the Fundamental Aeronautics Program at the NASA Glenn Research Center.

Level of Review: This material has been technically reviewed by technical management.

Available from

NASA Center for Aerospace Information
7121 Standard Drive
Hanover, MD 21076–1320

National Technical Information Service
5285 Port Royal Road
Springfield, VA 22161

Available electronically at http://gltrs.grc.nasa.gov

Three-Dimensional Field Solutions for Multi-Pole Cylindrical Halbach Arrays in an Axial Orientation

William K. Thompson
National Aeronautics and Space Administration
Glenn Research Center
Cleveland, Ohio 44135

1. Introduction

Uses for the so-called Halbach array of permanent magnets have grown in number in recent years. The salient feature of the Halbach array is the unique placement of individual permanent magnets such that the *B* field is concentrated on one side of the array and canceled on the other. This useful and intuitively efficient property exists for both linear and cylindrical arrays (ref. 1). In addition to the inventor's original designs for particle beam focusing mechanisms and undulators, one may now find Halbach arrays in a number of applications, including high-performance motors and generators (ref. 2), frictionless passive magnetic bearings and couplers (refs. 2 and 6) and magnetically levitated trains (ref. 3).

This article presents three-dimensional *B* field solutions for the cylindrical Halbach array in an axial orientation. This arrangement has applications in the design of axial motors and passive axial magnetic bearings and couplers. The analytical model described here assumes ideal magnets with fixed and uniform magnetization. The model also assumes a sufficiently large number of magnets ($N_m \geq 16$) comprise the Halbach array so that the angular span of each individual magnet is kept small. This permits modeling its magnetization as arising from a sum of four surface currents. The field component functions are expressed as sums of 2-D definite integrals that are easily computed by a number of mathematical analysis software packages. The solutions are found to be sinusoidal functions of angular position (with additional harmonics present at axial distances that are small compared to the magnet thickness), exponential functions of axial distance from the magnets and more complex functions of radial position that must be computed numerically. The analysis is verified with sample calculations and the results are compared to equivalent results from traditional finite-element analysis (FEA). The field solutions are then approximated for use in flux linkage and induced EMF calculations in nearby stator windings by expressing the field variance with angular displacement as pure sinusoidal function whose amplitude depends on radial and axial position. The primary advantage of numerical implementation of the analytical approach presented in the article is that it lends itself more readily to parametric analysis and design tradeoffs than traditional FEA models.

2. Magnetic Field Theory of The Axial Halbach Array

Figure 1 shows the cylindrical Halbach array in an axial orientation. The term "axial Halbach array" will be used from this point forward to refer to this configuration. The array depicted is comprised of $N_m = 32$ sector shaped permanent magnets with inner radius r_1, outer radius r_2, and axial thickness T. Assume that $N_m \geq 16$ so that the angle in radians spanned by each magnet is small compared with 2π. There are four magnets per Halbach wavelength in the angular (ϕ) direction. Each sector in the array has an index s, where $s = [0, 1, \ldots N_m\text{-}1]$. The magnets each have a magnetization $M = \pm B_r/\mu_o$ whose direction is indicated by the arrows. B_r is the remanent magnetization of the permanent magnet material.

Field calculations require the definition of two overlapping coordinate systems, one Cartesian and the other cylindrical. The cylindrical $r\phi$ plane aligns with the Cartesian xy plane, so that the z coordinates of each system are identical. The $+x$ axis of the Cartesian system lies at $\phi = 0$ in the cylindrical system. The field solutions will be found at any arbitrary point in space, which defines a vector in the cylindrical system given by $\vec{r} = (\mathrm{r}\,\hat{r} + \phi\hat{\phi} + \mathrm{z}\,\hat{z})$. The vector giving the location of the integration variable is

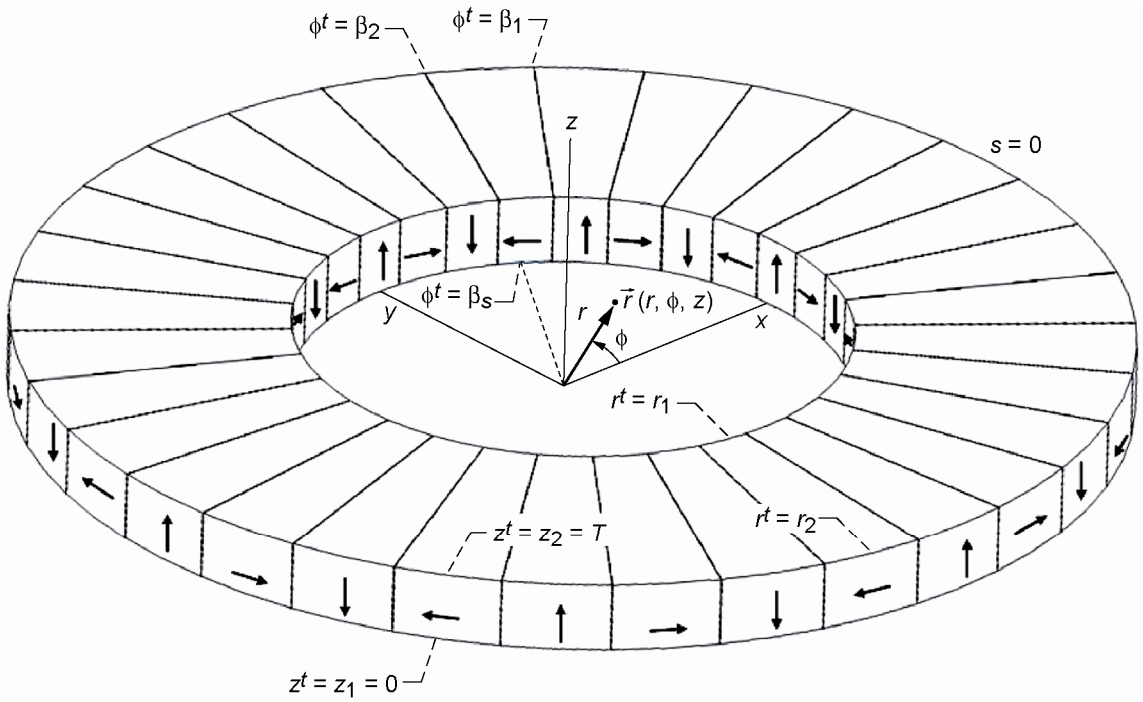

Figure 1.—The axial Halbach array for N_m = 32 magnets. Arrows indicate the direction of magnetization for each individual magnet. This particular arrangement will concentrate the *B* field below the ring and cancel it above the ring.

designated by primes, i.e., $\vec{r}\,' = (r'\hat{r} + \phi'\hat{\phi} + z'\hat{z})$. The distance between these two points is given by Green's function

$$G(\vec{r}, \vec{r}\,') = \frac{1}{|\vec{r} - \vec{r}\,'|} = \frac{1}{\sqrt{r^2 + r'^2 + (z - z')^2 - 2rr'\cos(\phi - \phi')}} \tag{1}$$

The array lies in the Cartesian system such that the +*z* axis corresponds to the axis of rotation and the flat bottom faces of the sectors lie in the *xy* plane. Hence, $z_1 = 0$ and $z_2 = T$. The $s = 0$ magnet is selected to be magnetized in the axial (+*z*) direction and the +*x* axis bisects the flat bottom surface of this magnet. Magnets lying on the –*x*, +*y*, and –*y* axes also bear this same direction of magnetization. The s^{th} magnet has a central radial axis which lies at angle $\phi = \beta_s = 2\pi s/N_m$. Each magnet subtends an angle in the ϕ direction of $\beta_2 - \beta_1 = 2\pi/N_m$ radians, where β_2 and β_1 are the locations of the side faces.

The magnetic field component solutions are expressed in cylindrical coordinates as

$$\vec{B}(r, \phi, z) = \{B_r, B_\phi, B_z\} \tag{2}$$

and these may be transformed to Cartesian coordinates using

$$\vec{B}(x, y, z) = \{B_r \cos\phi - B_\phi \sin\phi, \quad B_r \sin\phi + B_\phi \cos\phi, \quad B_z\} \tag{3}$$

Using the principle of linear superposition, one may express the aggregate field components as the sum of individual contributions from each sector in the array. For any axially magnetized (±*z*) magnet in the array, the *B* field components may be calculated from the vector potential and expressed as sums of definite integrals in two of the spatial dimensions as determined previously (ref. 4):

$$B_{r,a}(\vec{r}) = \pm\frac{\mu_o M}{4\pi}\sum_{j=1}^{2}(-1)^{j}\left\{\begin{array}{l}\left[\int_{z_1}^{z_2}\int_{\beta_1}^{\beta_2}\frac{(z-z')\cos(\phi-\phi')}{|\vec{r}-\vec{r}\,'|^3}r'\,d\phi'\,dz'\right]_{r'=r_j} + \\ \left[\int_{z_1}^{z_2}\int_{r_1}^{r_2}\frac{(z-z')\sin(\phi-\phi')}{|\vec{r}-\vec{r}\,'|^3}dr'\,dz'\right]_{\phi'=\beta_j}\end{array}\right\} \tag{4a}$$

$$B_{\phi,a}(\vec{r}) = \pm\frac{\mu_o M}{4\pi}\sum_{j=1}^{2}(-1)^{j+1}\left\{\begin{array}{l}\left[\int_{z_1}^{z_2}\int_{\beta_1}^{\beta_2}\frac{(z-z')\sin(\phi-\phi')}{|\vec{r}-\vec{r}\,'|^3}r'\,d\phi'\,dz'\right]_{r'=r_j} - \\ \left[\int_{z_1}^{z_2}\int_{r_1}^{r_2}\frac{(z-z')\cos(\phi-\phi')}{|\vec{r}-\vec{r}\,'|^3}dr'\,dz'\right]_{\phi'=\beta_j}\end{array}\right\} \tag{4b}$$

$$B_{z,a}(\vec{r}) = \pm\frac{\mu_o M}{4\pi}\sum_{j=1}^{2}(-1)^{j+1}\left\{\begin{array}{l}\left[\int_{z_1}^{z_2}\int_{\beta_1}^{\beta_2}\frac{r\cos(\phi-\phi')-r'}{|\vec{r}-\vec{r}\,'|^3}r'\,d\phi'\,dz'\right]_{r'=r_j} + \\ \left[\int_{z_1}^{z_2}\int_{r_1}^{r_2}\frac{r\sin(\phi-\phi')}{|\vec{r}-\vec{r}\,'|^3}dr'\,dz'\right]_{\phi'=\beta_j}\end{array}\right\} \tag{4c}$$

Note that $+M$ is used for $+z$ magnetization and $-M$ is used for $-z$ magnetization. In a similar manner, expressions for the field components for an individual transversely magnetized sector may be expressed in the following equations, which are derived in the appendix of this article.

$$B_{r,t}(\vec{r}) = \pm\frac{\mu_o M}{4\pi}\sum_{j=1}^{2}(-1)^{j+1}\left\{\begin{array}{l}\left[\int_{z_1}^{z_2}\int_{\beta_1}^{\beta_2}\frac{-\sin(\phi-\phi')}{|\vec{r}-\vec{r}\,'|^3}r'^2\,d\phi'\,dz'\right]_{r'=r_j} + \\ \left[\int_{r_1}^{r_2}\int_{\beta_1}^{\beta_2}\frac{\sin(\phi-\phi')(z-z')}{|\vec{r}-\vec{r}\,'|^3}r'\,d\phi'\,dr'\right]_{z'=z_j}\end{array}\right\} \tag{5a}$$

$$B_{\phi,t}(\vec{r}) = \pm\frac{\mu_o M}{4\pi}\sum_{j=1}^{2}(-1)^{j+1}\left\{\begin{array}{l}\left[\int_{r_1}^{r_2}\int_{\beta_1}^{\beta_2}\frac{\cos(\phi-\phi')(z-z')}{|\vec{r}-\vec{r}\,'|^3}r'\,d\phi'\,dr'\right]_{z'=z_j} + \\ \left[\int_{z_1}^{z_2}\int_{\beta_1}^{\beta_2}\frac{\left(r-r'\cos(\phi-\phi')\right)}{|\vec{r}-\vec{r}\,'|^3}r'\,d\phi'\,dz'\right]_{r'=r_j}\end{array}\right\} \tag{5b}$$

$$B_{z,t}(\vec{r}) = \pm\frac{\mu_o M}{4\pi}\sum_{j=1}^{2}(-1)^{j+1}\left\{\left[\int_{r_1}^{r_2}\int_{\beta_1}^{\beta_2}\frac{-r\sin(\phi-\phi')}{|\vec{r}-\vec{r}'|^3}r'\,d\phi'\,dr'\right]_{z'=z_j}\right\} \tag{5c}$$

Here the assumption of sufficiently large N_m becomes particularly important as the magnetization is not truly azimuthal but linear and perpendicular to the radial axis of the magnet at $\phi = \beta_s$. Note that $+M$ is used for $+\phi$ magnetization and $-M$ is used for $-\phi$ magnetization.

The contributions of each magnet in the array add to give the aggregate solution. Starting at the $s = 0$ magnet and traveling around the array in the $+\phi$ direction, the magnetization directions repeat the pattern $\{+\hat{z}, +\hat{\phi}, -\hat{z}, -\hat{\phi}, +\hat{z} \ \ldots\}$.

Therefore, the magnetizations for each sector in the array are

$$\text{Axial Case:} \quad \vec{M} = (-1)^n M\hat{z} \tag{6a}$$

$$\text{Transverse Case:} \quad \vec{M} = (-1)^n M\hat{\phi} \tag{6b}$$

A new indexing variable n has been defined to account for the interleaving of axially and transversely magnetized sectors. One may express the angular position of each axially magnetized sector as

$$\beta_s(n) = \frac{4n\pi}{N_m} \tag{7}$$

and the left and right faces of the sector correspond to angles at

$$\beta_1 = \frac{(4n-1)\pi}{N_m}, \qquad \beta_2 = \frac{(4n+1)\pi}{N_m} \tag{8}$$

Similarly, each transversely magnetized sector is located at an angular position

$$\beta_s(n) = \frac{(4n+2)\pi}{N_m} \tag{9}$$

and the left and right faces of the sector correspond to angles

$$\beta_1 = \frac{(4n+1)\pi}{N_m}, \qquad \beta_2 = \frac{(4n+3)\pi}{N_m} \tag{10}$$

this yields the field components for the entire collection as

$$B_r(\vec{r}) = \frac{\mu_o M}{4\pi} \sum_{n=0}^{\frac{N_m}{2}-1} (-1)^n \sum_{j=1}^{2} (-1)^j \left[\begin{array}{l} \left[\int_{z_1}^{z_2} \int_{\beta_1=\frac{(4n-1)\pi}{N_m}}^{\beta_2=\frac{(4n+1)\pi}{N_m}} \frac{(z-z')\cos(\phi-\phi')}{|\vec{r}-\vec{r}'|^3} r' \, d\phi' \, dz' \right]_{r'=r_j} + \\ \left[\int_{z_1}^{z_2} \int_{r_1}^{r_2} \frac{(z-z')\sin(\phi-\phi')}{|\vec{r}-\vec{r}'|^3} dr' \, dz' \right]_{\phi'=\beta_j=\frac{(4n+2j-3)\pi}{N_m}} + \\ \left[\int_{z_1}^{z_2} \int_{\beta_1=\frac{(4n+1)\pi}{N_m}}^{\beta_2=\frac{(4n+3)\pi}{N_m}} \frac{\sin(\phi-\phi')}{|\vec{r}-\vec{r}'|^3} r'^2 \, d\phi' \, dz' \right]_{r'=r_j} - \\ \left[\int_{r_1}^{r_2} \int_{\beta_1=\frac{(4n+1)\pi}{N_m}}^{\beta_2=\frac{(4n+3)\pi}{N_m}} \frac{(z-z')\sin(\phi-\phi')}{|\vec{r}-\vec{r}'|^3} r' \, d\phi' \, dr' \right]_{z'=z_j} \end{array} \right] \tag{11a}$$

$$B_\phi(\vec{r}) = \frac{\mu_o M}{4\pi} \sum_{n=0}^{\frac{N_m}{2}-1} (-1)^n \sum_{j=1}^{2} (-1)^{j+1} \left[\begin{array}{l} \left[\int_{z_1}^{z_2} \int_{\beta_1=\frac{(4n-1)\pi}{N_m}}^{\beta_2=\frac{(4n+1)\pi}{N_m}} \frac{(z-z')\sin(\phi-\phi')}{|\vec{r}-\vec{r}'|^3} r' \, d\phi' \, dz' \right]_{r'=r_j} - \\ \left[\int_{z_1}^{z_2} \int_{r_1}^{r_2} \frac{(z-z')\cos(\phi-\phi')}{|\vec{r}-\vec{r}'|^3} dr' \, dz' \right]_{\phi'=\beta_j=\frac{(4n+2j-3)\pi}{N_m}} + \\ \left[\int_{r_1}^{r_2} \int_{\beta_1=\frac{(4n+1)\pi}{N_m}}^{\beta_2=\frac{(4n+3)\pi}{N_m}} \frac{(z-z')\cos(\phi-\phi')}{|\vec{r}-\vec{r}'|^3} r' \, d\phi' \, dr' \right]_{z'=z_j} + \\ \left[\int_{z_1}^{z_2} \int_{\beta_1=\frac{(4n+1)\pi}{N_m}}^{\beta_2=\frac{(4n+3)\pi}{N_m}} \frac{(r-r'\cos(\phi-\phi'))}{|\vec{r}-\vec{r}'|^3} r' \, d\phi' \, dz' \right]_{r'=r_j} \end{array} \right] \tag{11b}$$

$$B_z(\vec{r}) = \frac{\mu_o M}{4\pi} \sum_{n=0}^{\frac{N_m}{2}-1} (-1)^n \sum_{j=1}^{2} (-1)^{j+1} \left[\begin{array}{l} \left[\int_{z_1}^{z_2} \int_{\beta_1=\frac{(4n-1)\pi}{N_m}}^{\beta_2=\frac{(4n+1)\pi}{N_m}} \frac{r\cos(\phi-\phi')-r'}{|\vec{r}-\vec{r}'|^3} r' \, d\phi' \, dr' \right]_{r'=r_j} + \\ \left[\int_{z_1}^{z_2} \int_{r_1}^{r_2} \frac{r\sin(\phi-\phi')}{|\vec{r}-\vec{r}'|^3} dr' \, dz' \right]_{\phi'=\beta_j=\frac{(4n+2j-3)\pi}{N_m}} - \\ \left[\int_{r_1}^{r_2} \int_{\beta_1=\frac{(4n+1)\pi}{N_m}}^{\beta_2=\frac{(4n+3)\pi}{N_m}} \frac{r\sin(\phi-\phi')}{|\vec{r}-\vec{r}'|^3} r' \, d\phi' \, dr' \right]_{z'=z_j} \end{array} \right] \tag{11c}$$

These expressions define the *B* field components at any point in space. They may be easily implemented in a variety of commercial mathematical analysis software packages. We used *Mathematica v5.2* (Wolfram Research, Inc). Special care must be taken to observe the signs of each of the terms, which are dictated by the *j* variable of summation.

3. Results and Validation of Field Solutions

The analytical expressions for the *B* field components given in section 2 have been coded in *Mathematica*. This product permits easy numerical implementation of the definite integrals using the built-in **NIntegrate[]** function. The working precision for the numerical integrations was set to 50 digits and the accuracy goal to five decimal places. Equivalent FEA models were also developed in *Maxwell 3D v10* (Ansoft, Inc.). The validation method compares the results of these two independent models of the same axial Halbach array.

The selected design parameters for the simulations are:

r_1 = 1.0" (25.4 mm), r_2 = 2.0" (50.8 mm)
$T = z_2 - z_1$ = 0.25" (6.4 mm)
N_m = 32 magnets, 4 magnets per Halbach wavelength
$B_r = \mu_o M$ = 1.5 T (NdFeB-55 rare earth permanent magnets)

These parameters match those of an axial magnetic bearing model currently under development at NASA Glenn Research Center (ref. 5).

Figures 2(a), (b), and (c) compare the radial, angular and axial dependence, respectively, of the B_r component of the analytical and FEA models at an axial gap distance z = –0.05 in. (–1.3 mm).

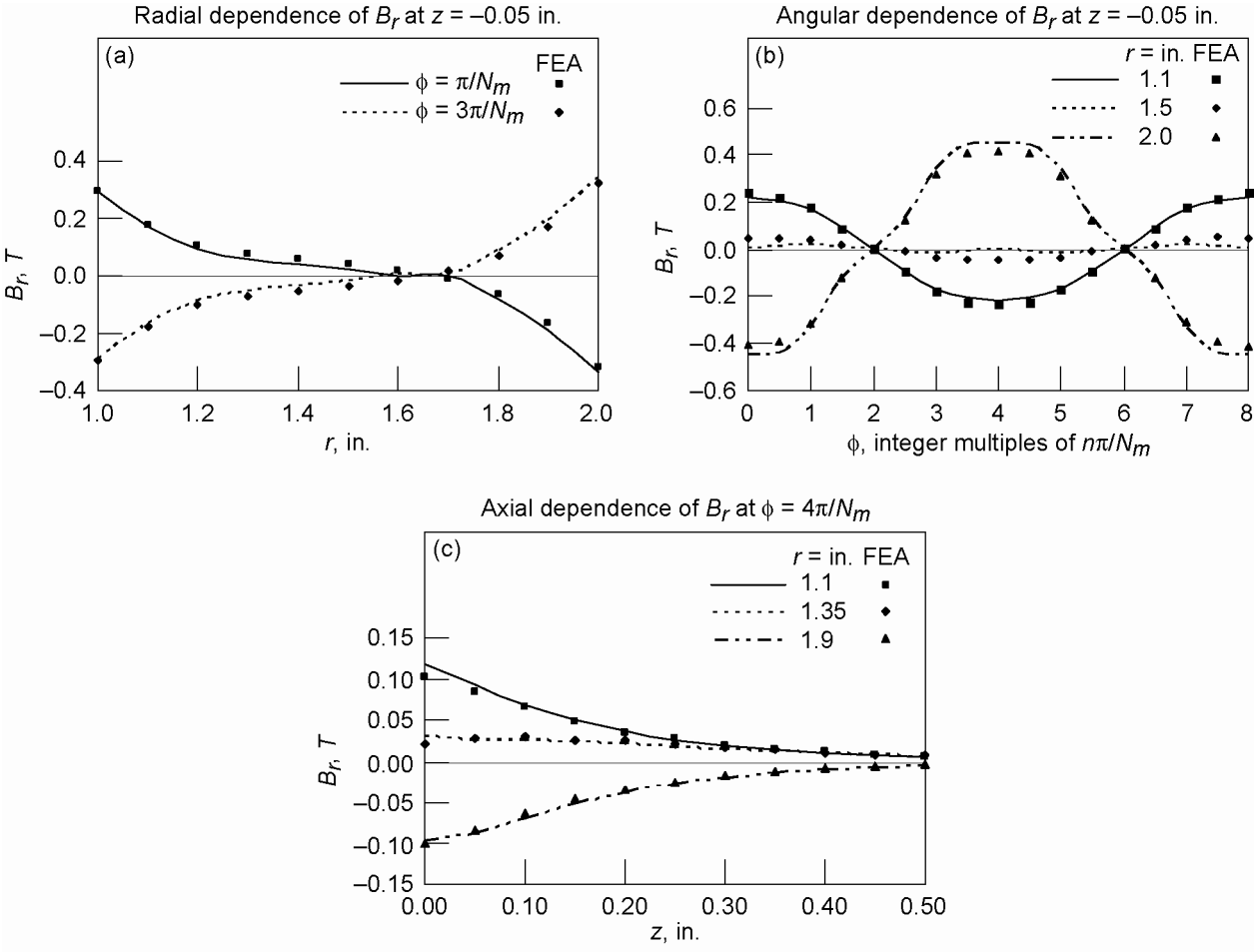

Figure 2.—Axial Halbach array at selected radial and axial distances and angular locations. Results of numerical integration of the analytical expressions are shown as smoothed lines. Equivalent FEA results are shown as markers at selected points. (a) B_r versus r. (b) B_r versus ϕ. (c) B_r versus z.

Figures 3(a), (b), and (c) compare the radial, angular and axial dependence of the B_ϕ component of the analytical and FEA models at an axial gap distance of z = –0.05 in. (–1.3 mm). Figures 4(a), (b), and (c) compare the radial, angular and axial dependence of the B_z component of the analytical and FEA models at an axial gap distance of z = –0.05 in. (–1.3 mm). Figures 5(a), (b), and (c) plot the three B field components in the first quadrant of the xy plane at an axial gap distance of z = –0.05 in. (–1.3 mm). Finally, Figure 6 compares the azimuthal dependence of the three B field components at a larger gap distance of z = –0.15 in. (–3.8 mm) and at the radial location which produces the maximum field: r = 1.35 in. (34 mm).

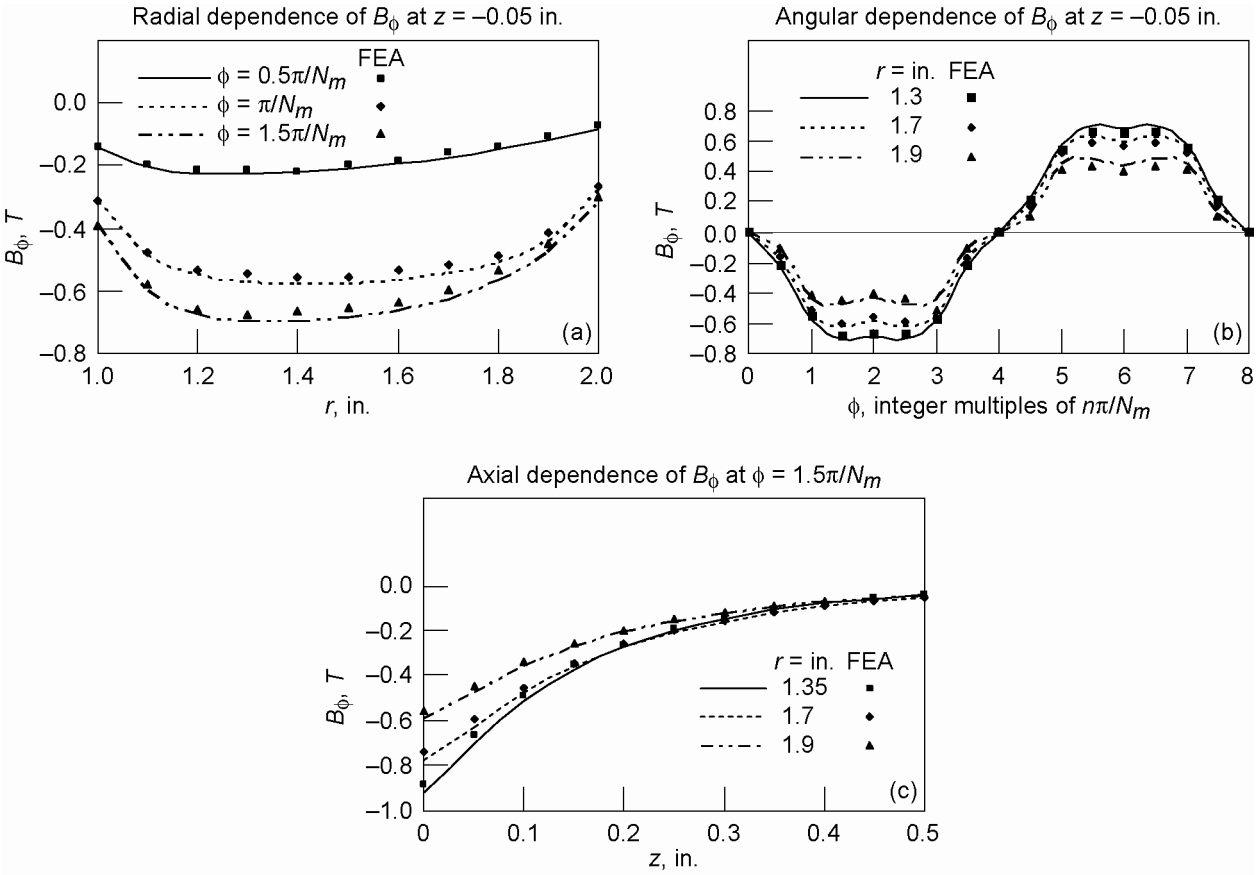

Figure 3.—Axial Halbach array at selected radial and axial distances and angular locations. Results of numerical integration of the analytical expressions are shown as smoothed lines. Equivalent FEA results are shown as markers at selected points. (a) B_r versus r. (b) B_r versus ϕ. (c) B_r versus z.

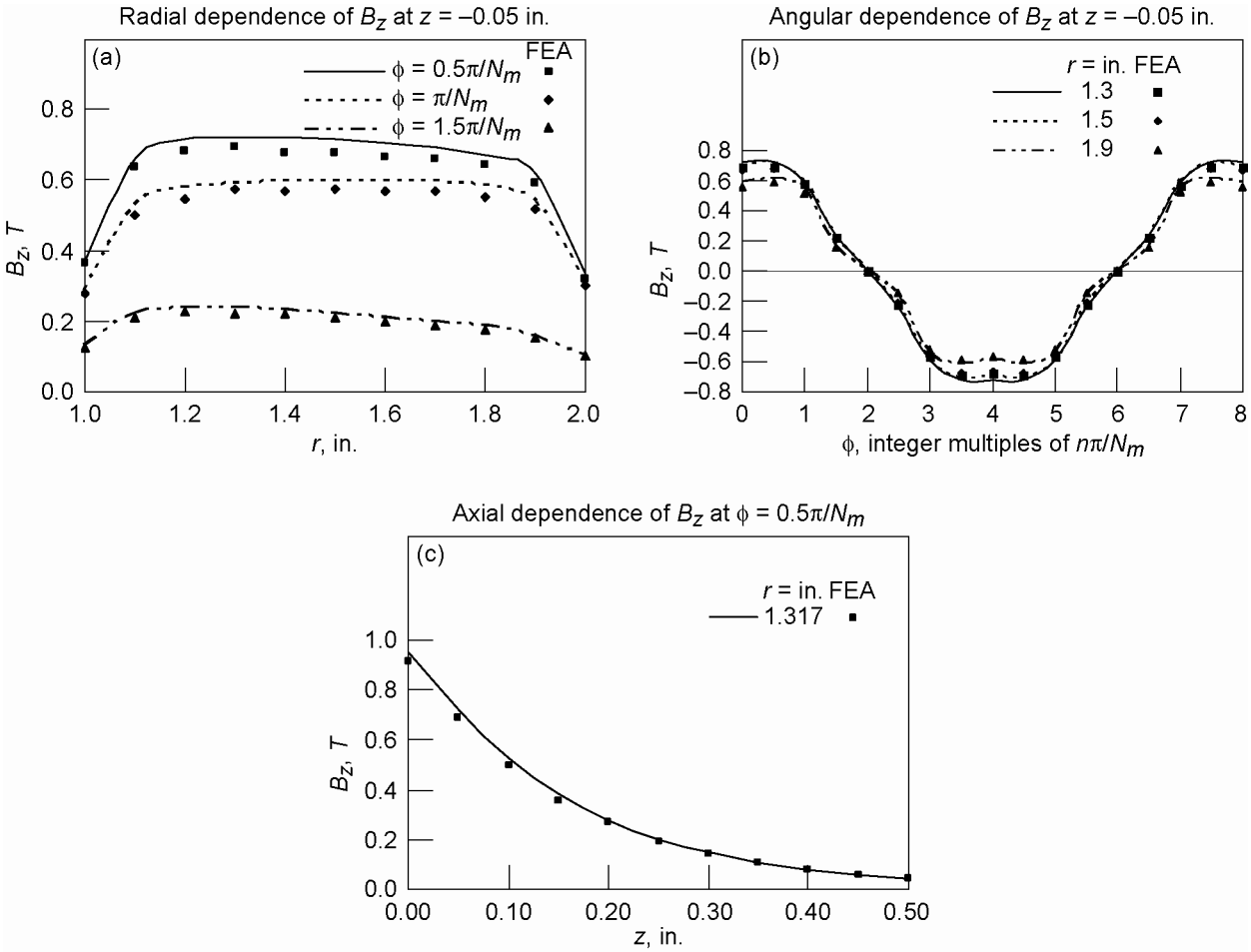

Figure 4.—Axial Halbach array at selected radial and axial distances and angular locations. Results of numerical integration of the analytical expressions are shown as smoothed lines. Equivalent FEA results are shown as markers at selected points. (a) B_z versus r. (b) B_z versus ϕ. (c) B_z versus z.

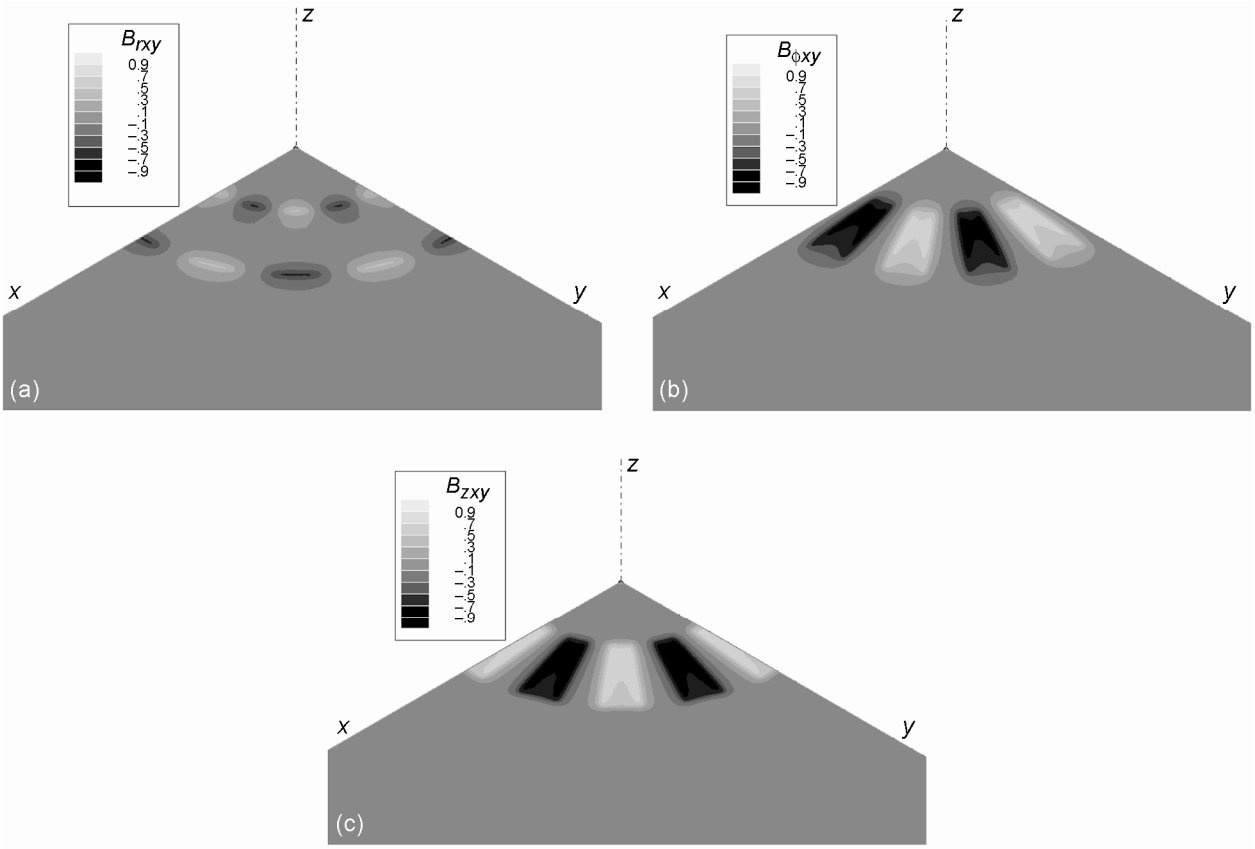

Figure 5.—3D plots of FEA results for B field components B_r (a), B_ϕ (b) and B_z (c) of the axial Halbach array in the first quadrant of the r_ϕ plane at an axial distance of z = –0.03 in. below the magnets.

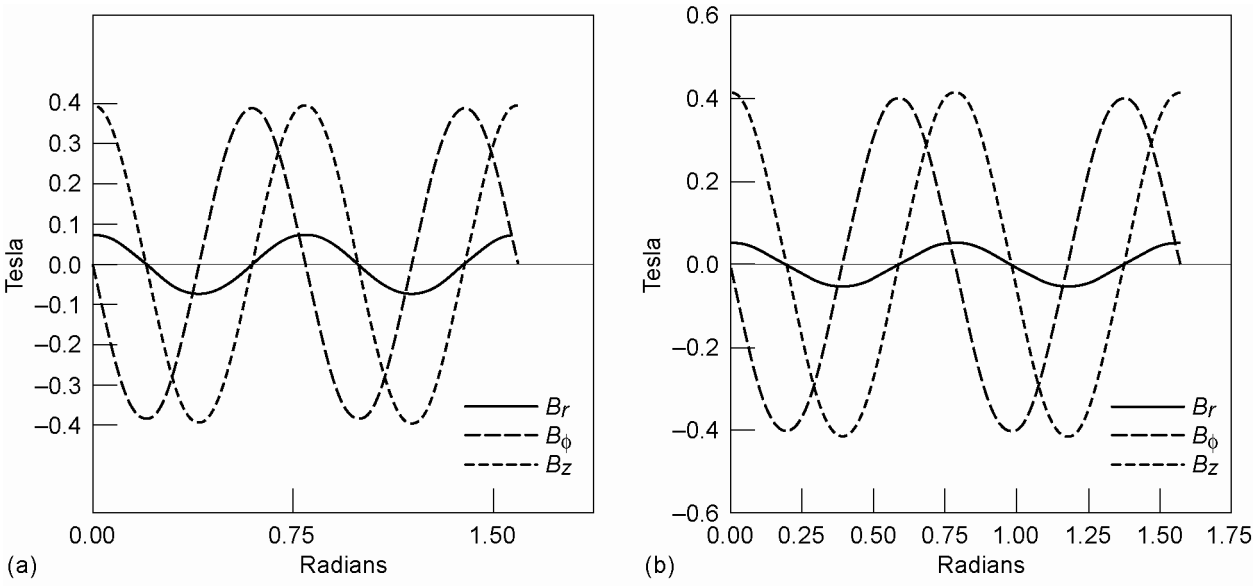

Figure 6.— 2D plots of B_r, B_ϕ and B_Z versus angular position (ϕ) at r = 1.35 in. (34 mm) and z = –0.15 in. (4 mm) as computed by FEA (a) and analytical (b) models. Both models indicate that at sufficiently large values of gap (g) the field components exhibit nearly perfect sinusoidal behavior with negligible harmonic components.

4. Discussion

The plots indicate agreement to within 10 percent of peak values between the numerical implementation of the analytical model presented in this article and an equivalent FEA model. The radial component of the field B_r is the weakest of the three and has significant magnitude only at the two radial edges of the array. For most practical applications, this field component is of no consequence.

Both the B_ϕ and B_z components have higher amplitude and greater spatial extent and achieve their maximum amplitudes at radial distances r = 1.35 in. (34 mm) and r = 1.317 in. (33.5 mm), respectively. The B_z component is flatter than B_ϕ over the radial extent of the magnets, as can be seen by comparing Figures 4(a) and 5(a). However, both B_ϕ and B_z must be treated as functions of radial position, $B_\phi(r)$ and $B_z(r)$ when computing flux linkage and induced emf and current in nearby stator windings.

At gap values which are small compared to the magnet thickness, T, all three field components contain significant harmonics versus angular position ϕ. The angular frequency of the fundamental is $\omega_1 = 8\pi/N_m$ as can be seen from figures 3(b), 4(b), and 5(b). At an axial position of z = –0.05 in. (–1.3 mm) distortion of the sinusoid arises mostly from a 5th harmonic. As $z \rightarrow 0$ one finds the presence of even higher order harmonics. However, for most practical applications the field is used to compute flux linkage in a winding of relatively large spatial extent where the gap is sufficiently large such that all harmonic content may be neglected. For larger values of z, only the fundamental sinusoid of frequency f_1 remains as shown in figure 7. Here the gap value is –0.15 in. (–3.8 mm).

Post has determined that the axial dependence of the field components is an exponential function (ref. 3) of the form $B = B_o\, e^{-kz}$ where $k = 2\pi/\lambda$ and λ is the Halbach wavelength, i.e., the width of four magnets along the direction of travel. For the axial Halbach array, the direction of travel is azimuthal and k is not a constant as in (ref. 3) but a function of radial position given by

$$k(r) = N_m/4r \tag{11}$$

Summarizing all of this, we can write field component equations in the manner described by Post (ref. 3) using the form

$$B_\phi = B_{\phi o} \sin\phi\, e^{-kz} \tag{12a}$$

$$B_z = B_{zo} \cos\phi\, e^{-kz} \tag{12b}$$

with the understanding that the $B_{\phi o}$, B_{zo} and k are all functions of r. $B_{\phi o}$, and B_{zo} give the field component strengths of the fundamental at the surface of the Halbach magnet array (z = 0) and at radial location r. This gives

$$B_\phi(r,\phi,z) = B_{\phi o}(r) \sin\phi\, e^{-k(r)z} \tag{13a}$$

$$B_z(r,\phi,z) = B_{zo}(r) \cos\phi\, e^{-k(r)z} \tag{13b}$$

as the working equations for the axial Halbach array. From these, dynamic analysis of a rotating array may follow by substituting $\phi = \phi_i - \omega t$, where ϕ_i is the initial angular position of the array and ω is the mechanical frequency of rotation. The analysis is simplified if the array is initially positioned with $\phi_i = 0$. Dynamic analysis is explored further in a related article (ref. 5).

Furthermore, simplifying assumptions may be made regarding the effect of relatively distant magnets from the spatial location of interest. The field effects of magnets more than two Halbach wavelengths away from a spatial location near the array may be considered negligible. Factoring this into the

programming of the numerical computation of the analytical model may reduce computation times drastically, especially for very large N_m. Finally, in a related article (ref. 6) Post simplifies further by assuming an average value over the span of a nearby stator winding for the peak field, rather than the function of radial position indicated above. This produces a closed form approximation to the field that may be sufficiently accurate for a variety of applications.

5. Conclusion

This article presents analytical expressions for the B field solutions for an axial Halbach array of permanent magnets. The analytical expressions are easily implemented in numerical analysis software packages. Validation of the analytical model by finite element analysis shows agreement between the two methods within 10 percent of the peak value of the field.

Appendix

Derivation of *B* Field Solutions for Transversely Magnetized Sector Magnets

A sector of permanent magnetic material with inner radius r_1 and outer radius r_2 is positioned such that the center axis of the bottom surface coincides with an azimuthal angle ($\phi = \beta_s$) and the bottom face of the sector lies in the *xy* plane (z_1=0). Although only field effects from a single sector are considered here, the sector is known to be part of a complete circular array of N_m identically-sized magnets and therefore subtends an angle $\beta = 2\pi/N_m$. The angular component ϕ is defined over the range $[0, 2\pi]$.

We proceed with the derivation of $\vec{B}$ via the vector potential $\vec{A}$ in a similar method as Furlani (ref. 4). Figure 7 shows the geometry of the magnetization in terms of the spatial integration variables r', ϕ' and z'. The magnetization vector ***M*** lies in the transverse plane. For a sufficiently large number of magnets in the total array, the angle subtended by each individual magnet is small. In this case the magnetization may be approximated as having a $\hat{\phi}$ component only, given by

$$\vec{M} = \pm M\hat{\phi} \tag{14}$$

since $\vec{J} = \nabla \times \vec{M}$ and the magnetization has no net circulation, there is no volume current density. The magnetization therefore arises from surface current densities on the top, bottom, inner and outer surfaces of the magnet sector, where

$$\vec{j}_M = \vec{M} \times \hat{n} \tag{15}$$

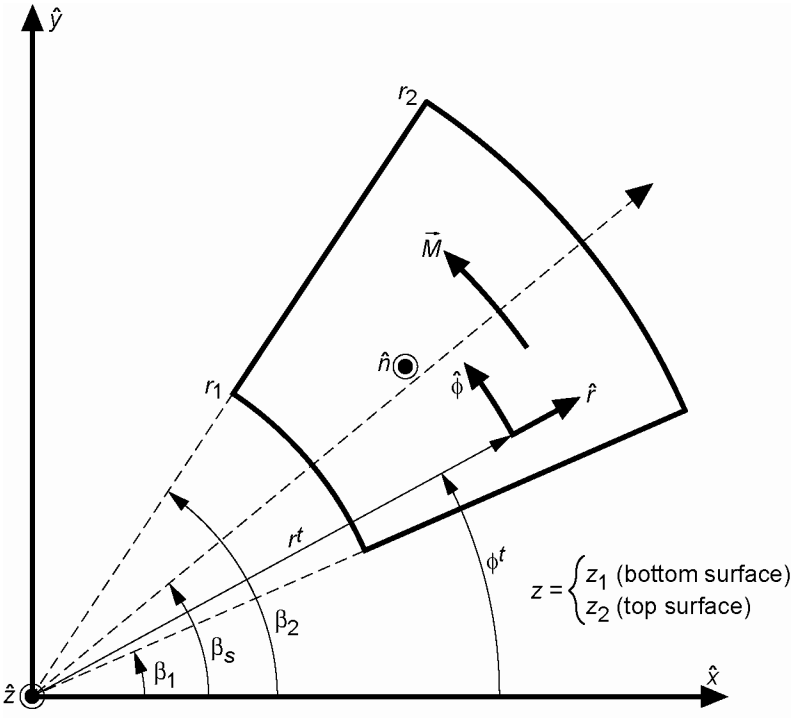

Figure 7.—Coordinate systems for the derivation of the component *B* field expressions for a single transversely magnetized sector at an angular position, β_s. *M* points in the direction of $\hat{\phi}$ at the centerline of the sector, where $\phi = \beta_s$. Primed quantities indicate variables of integration.

The four surfaces are described analytically as

$$top\ surface = \begin{cases} r_1 \le r' \le r_2 \\ \beta_1 \le \phi' \le \beta_2 \\ z' = z_2 \end{cases} \tag{16a}$$

$$bottom\ surface = \begin{cases} r_1 \le r' \le r_2 \\ \beta_1 \le \phi' \le \beta_2 \\ z' = z_1 \end{cases} \tag{16b}$$

$$inner\ surface = \begin{cases} r' = r_1 \\ \beta_1 \le \phi' \le \beta_2 \\ z_1 \le z' \le z_2 \end{cases} \tag{16c}$$

$$outer\ surface = \begin{cases} r' = r_2 \\ \beta_1 \le \phi' \le \beta_2 \\ z_1 \le z' \le z_2 \end{cases} \tag{16d}$$

The four surface normals are given by

$$\hat{n} = \begin{cases} +\hat{z} & (top) \\ -\hat{z} & (bottom) \\ -\hat{r} & (inner) \\ +\hat{r} & (outer) \end{cases} \tag{17}$$

and the four surface current densities are given by

$$\vec{j}_M = \begin{cases} M\hat{r} & (top) \\ -M\hat{r} & (bottom) \\ M\hat{z} & (inner) \\ -M\hat{z} & (outer) \end{cases} \tag{18}$$

We will derive B from the vector potential function, A, using

$$\vec{B} = \nabla \times \vec{A} \tag{19}$$

and Green's function

$$G(\vec{r}, \vec{r}\,') = \frac{1}{|\vec{r} - \vec{r}\,'|} = \frac{1}{\sqrt{r^2 + r'^2 + (z - z')^2 - 2rr'\cos(\phi - \phi')}} \tag{20}$$

which gives the distance between the spatial location of interest and the variables of integration. The vector potential arises from volume and surface current densities, but the volume density has already been

shown to be zero. Therefore the vector potential will arise from four surface integrals of surface current densities given by

$$A(\vec{r}) = \frac{\mu_o}{4\pi} \int_S \frac{j_M(\vec{r})}{|\vec{r} - \vec{r}'|} da' \tag{21}$$

Substituting equation (16) into this expression for j_M gives

$$A_s(\vec{r}) = \pm \frac{\mu_o M}{4\pi} \sum_{j=1}^{2} (-1)^j \left\{ \left[\int_{r_1}^{r_2} \int_{\beta_1}^{\beta_2} \frac{\hat{r}}{|\vec{r} - \vec{r}'|} r' d\phi' dr' \right]_{z'=z_j} - \left[\int_{z_1}^{z_2} \int_{\beta_1}^{\beta_2} \frac{\hat{z}}{|\vec{r} - \vec{r}'|} r' d\phi' dz' \right]_{r'=r_j} \right\} \tag{22}$$

but $\hat{r}$ is a function of the angular position variable ϕ'. Substituting the transformation

$$\hat{r} = \cos\phi' \hat{x} + \sin\phi' \hat{y} \tag{23}$$

and arranging terms gives

$$A_s(\vec{r}) = \pm \frac{\mu_o M}{4\pi} \sum_{j=1}^{2} (-1)^j \left\{ \begin{array}{l} \left[\int_{r_1}^{r_2} \int_{\beta_1}^{\beta_2} \frac{\cos\phi' \hat{x}}{|\vec{r} - \vec{r}'|} r' d\phi' dr' \right]_{z'=z_j} + \\ \left[\int_{r_1}^{r_2} \int_{\beta_1}^{\beta_2} \frac{\sin\phi' \hat{y}}{|\vec{r} - \vec{r}'|} r' d\phi' dr' \right]_{z'=z_j} - \\ \left[\int_{z_1}^{z_2} \int_{\beta_1}^{\beta_2} \frac{\hat{z}}{|\vec{r} - \vec{r}'|} r' d\phi' dz' \right]_{r'=r_j} \end{array} \right\} \tag{24}$$

which is the vector potential at the point of interest in terms of the Cartesian unit vectors. Projecting these terms back into cylindrical coordinates using

$$\hat{x} = \cos\phi \hat{r} - \sin\phi \hat{\phi} \tag{25a}$$

$$\hat{y} = \sin\phi \hat{r} + \cos\phi \hat{\phi} \tag{25b}$$

one may collect like terms and simplify using angle sum and difference trigonometric identities to obtain the cylindrical coordinate components of the vector potential function as

$$A_{r,s}(\vec{r}) = \pm \frac{\mu_o M}{4\pi} \sum_{j=1}^{2} (-1)^{j+1} \left\{ \left[\int_{r_1}^{r_2} \int_{\beta_1}^{\beta_2} \frac{-\cos(\phi - \phi')}{|\vec{r} - \vec{r}'|} r' d\phi' dr' \right]_{z'=z_j} \right\} \tag{26a}$$

$$A_{\phi,s}(\vec{r}) = \pm\frac{\mu_o M}{4\pi}\sum_{j=1}^{2}(-1)^{j+1}\left\{\left[\int_{r_1}^{r_2}\int_{\beta_1}^{\beta_2}\frac{\sin(\phi-\phi')}{|\vec{r}-\vec{r}\,'|}r'\,d\phi'\,dr'\right]_{z'=z_j}\right\} \tag{26b}$$

$$A_{z,s}(\vec{r}) = \pm\frac{\mu_o M}{4\pi}\sum_{j=1}^{2}(-1)^{j+1}\left[\int_{z_1}^{z_2}\int_{\beta_1}^{\beta_2}\frac{1}{|\vec{r}-\vec{r}\,'|}r'\,d\phi'\,dz'\right]_{r'=r_j} \tag{26c}$$

and the final step is to take the curl of A in cylindrical coordinates to obtain the individual components of the B field.

$$B_{r,s}(\vec{r}) = \frac{1}{r}\frac{\partial}{\partial\phi}A_{z,s}(\vec{r}) - \frac{\partial}{\partial z}A_{\phi,s}(\vec{r}) = \pm\frac{\mu_o M}{4\pi}\sum_{j=1}^{2}(-1)^{j+1}\left\{\begin{array}{l}\left[\int_{z_1}^{z_2}\int_{\beta_1}^{\beta_2}\frac{-\sin(\phi-\phi')}{|\vec{r}-\vec{r}\,'|^3}r'^2\,d\phi'\,dz'\right]_{r'=r_j} + \\ \left[\int_{r_1}^{r_2}\int_{\beta_1}^{\beta_2}\frac{\sin(\phi-\phi')(z-z')}{|\vec{r}-\vec{r}\,'|^3}r'\,d\phi'\,dr'\right]_{z'=z_j}\end{array}\right\} \tag{27a}$$

$$B_{\phi,s}(\vec{r}) = \frac{\partial}{\partial z}A_{r,s}(\vec{r}) - \frac{\partial}{\partial r}A_{z,s}(\vec{r}) = \pm\frac{\mu_o M}{4\pi}\sum_{j=1}^{2}(-1)^{j+1}\left\{\begin{array}{l}\left[\int_{r_1}^{r_2}\int_{\beta_1}^{\beta_2}\frac{\cos(\phi-\phi')(z-z')}{|\vec{r}-\vec{r}\,'|^3}r'\,d\phi'\,dr'\right]_{z'=z_j} + \\ \left[\int_{z_1}^{z_2}\int_{\beta_1}^{\beta_2}\frac{\left(r-r'\cos(\phi-\phi')\right)}{|\vec{r}-\vec{r}\,'|^3}r'\,d\phi'\,dz'\right]_{r'=r_j}\end{array}\right\} \tag{27b}$$

$$B_{z,s}(\vec{r}) = \frac{1}{r}\left[\frac{\partial}{\partial r}(rA_{\phi,s}(\vec{r})) - \frac{\partial}{\partial\phi}A_{r,s}(\vec{r})\right] = \pm\frac{\mu_o M}{4\pi}\sum_{j=1}^{2}(-1)^{j+1}\left\{\left[\int_{r_1}^{r_2}\int_{\beta_1}^{\beta_2}\frac{-r\sin(\phi-\phi')}{|\vec{r}-\vec{r}\,'|^3}r'\,d\phi'\,dr'\right]_{z'=z_j}\right\} \tag{27c}$$

References

1. Halbach, K., "Design of permanent magnet multipole magnets with oriented rare earth cobalt material," *Nuclear Instruments and Methods*, vol. 169, 1980, pp. 1–l0.
2. Zhu, Z.Q. and Howe, D., "Halbach permanent magnet machines and applications: a review," *IEE Proc.-Electr. Power Appl.*, vol. 148, no. 4, July 2001, pp. 299–308.
3. Post, R.F. and Ryutov, D.D., "The Inductrack, a simpler approach to magnetic levitation," *IEEE Trans. Appl. Supercond.*, vol. 10(1), March 2000, pp. 901–4.
4. Furlani, E.P., "A three-dimensional field solution for axially polarized multipole disks," *J. Magn. Magn. Mater.*, vol. 135, 1994, pp. 205–214.
5. Eichenberg, D.J., Gallo, C.A., and Thompson, W.K., "Development and Testing of an Axial Halbach Magnetic Bearing," NASA/TM—2006-214357.
6. Post, R.F and Ryutov, D.D, "Ambient Temperature Passive Magnetic Bearings: Theory and Design Equations," Lawrence Livermore National Laboratory Publ. no. 232382, 1997.

REPORT DOCUMENTATION PAGE

Form Approved
OMB No. 0704-0188

1. AGENCY USE ONLY (*Leave blank*)	2. REPORT DATE	3. REPORT TYPE AND DATES COVERED
	September 2006	Technical Memorandum

4. TITLE AND SUBTITLE

Three-Dimensional Field Solutions for Multi-Pole Cylindrical Halbach Arrays in an Axial Orientation

5. FUNDING NUMBERS

WBS 561581.02.08.03.06.04

6. AUTHOR(S)

William K. Thompson

7. PERFORMING ORGANIZATION NAME(S) AND ADDRESS(ES)

National Aeronautics and Space Administration
John H. Glenn Research Center at Lewis Field
Cleveland, Ohio 44135–3191

8. PERFORMING ORGANIZATION REPORT NUMBER

E–15634

9. SPONSORING/MONITORING AGENCY NAME(S) AND ADDRESS(ES)

National Aeronautics and Space Administration
Washington, DC 20546–0001

10. SPONSORING/MONITORING AGENCY REPORT NUMBER

NASA TM—2006-214359

11. SUPPLEMENTARY NOTES

Responsbile person, William K. Thompson, organization code DEI, 216–433–2638.

12a. DISTRIBUTION/AVAILABILITY STATEMENT

Unclassified - Unlimited
Subject Categories: 07 and 70

Available electronically at http://gltrs.grc.nasa.gov

This publication is available from the NASA Center for AeroSpace Information, 301–621–0390.

12b. DISTRIBUTION CODE

13. ABSTRACT ***(Maximum 200 words)***

This article presents three-dimensional *B* field solutions for the cylindrical Halbach array in an axial orientation. This arrangement has applications in the design of axial motors and passive axial magnetic bearings and couplers. The analytical model described here assumes ideal magnets with fixed and uniform magnetization. The field component functions are expressed as sums of 2-D definite integrals that are easily computed by a number of mathematical analysis software packages. The analysis is verified with sample calculations and the results are compared to equivalent results from traditional finite-element analysis (FEA). The field solutions are then approximated for use in flux linkage and induced EMF calculations in nearby stator windings by expressing the field variance with angular displacement as pure sinusoidal function whose amplitude depends on radial and axial position. The primary advantage of numerical implementation of the analytical approach presented in the article is that it lends itself more readily to parametric analysis and design tradeoffs than traditional FEA models.

14. SUBJECT TERMS	15. NUMBER OF PAGES
Magnetic bearings; Levitation; Magnetic materials; Permanent magnets; Magnetic field	21
	16. PRICE CODE

17. SECURITY CLASSIFICATION OF REPORT	18. SECURITY CLASSIFICATION OF THIS PAGE	19. SECURITY CLASSIFICATION OF ABSTRACT	20. LIMITATION OF ABSTRACT
Unclassified	Unclassified	Unclassified	